ADVANCED OPTICAL MATERIALS
www.advopticalmat.de

Cluster and Kill: the Use of Clustering-Triggered Emission Materials for Singlet Oxygen Photosensitization in Antimicrobial Photodynamic Therapy

Karina Dueñas-Parro, Oscar Gulias, Montserrat Agut, Felipe de la de la Cruz-Martínez, Agustín Lara-Sánchez, José A. Castro-Osma, Juan F. García-Reyes, Antonio Sánchez-Ruiz, Cristina Martín, Santi Nonell,* and Roger Bresolí-Obach**

The emergence of light-based technologies is revolutionizing modern medicine and healthcare by enabling precise disease diagnosis and treatment through various luminescent agents and imaging techniques. Despite challenges like biocompatibility, spectral tuning, and synthesis complexity, the primary issue is the aggregation-caused quenching of emission on high concentrations or physiological conditions. In light of these problems, Clustering-Triggered Emission (CTE), which involves the formation of atomic clusters to induce light absorption and the luminescence of unconventional chromophores, represents an all-in-one solution to the challenges identified. Given the potential for CTE materials to behave in ways previously only associated with conventional chromophores, it seems reasonable that highly oxidative reactive oxygen species can be formed from CTE excited states. The results demonstrate that it is possible to transfer the excess energy from the CTE long-lived excited states to molecular oxygen, thereby producing singlet oxygen. It is also noteworthy that over 99.9% of *Staphylococcus aureus* cells can be eradicated using fluences comparable to those used in traditional systems under violet light irradiation. Uncovering these photophysical properties of CTE opens the door to a revolutionary breakthrough that can disrupt conventional photodynamic therapy and usher in a new era of CTE-based photosensitizers.

1. Introduction

Health has been a crucial aspect of human progress since ancient times. Serious diseases, particularly infectious ones, can lead to pandemic scenarios that significantly impact human civilization's economic, political, and social aspects.[1] In a world with an aging and infection-prone population, tackling infectious diseases and the hurdle of antimicrobial resistance is imperative.[2] That's why, in 2017, the World Health Organization (WHO) published its first list of "priority pathogens" for antibiotic research and development.[3] The aim is to develop new antimicrobial agents that effectively combat infections while minimizing resistance to them.[4,5]

In this context, photodynamic therapy (PDT) has been proposed as an alternative therapy to overcome antibiotic resistance. PDT is a non-invasive form of phototherapy,[6] that uses harmless light to activate non or low-toxic photosensitive

K. Dueñas-Parro, S. Nonell, R. Bresolí-Obach
Department de Química Analítica i aplicada
Institut Químic de Sarrià – Universitat Ramon Llull
Via Augusta 390, Barcelona 08017, Spain
E-mail: santi.nonell@iqs.url.edu; roger.bresoli@iqs.url.edu
O. Gulias, M. Agut
Departament de Bioenginyeria
Institut Químic de Sarrià – Universitat Ramon Llull
Via Augusta 390, Barcelona 08017, Spain
The ORCID identification number(s) for the author(s) of this article can be found under https://doi.org/10.1002/adom.202402179

DOI: 10.1002/adom.202402179

F. de la de la Cruz-Martínez, A. Lara-Sánchez, J. A. Castro-Osma
Departamento de Química Inorgánica
Orgánica y Bioquímica-Centro de Innovación de Química Avanzada (ORFEO-CINQA)
Facultad de Ciencias y Tecnologías Químicas Universidad de Castilla-la ManchaAvda
Camilo José Cela, 10, Ciudad Real 13071, Spain
J. F. García-Reyes
Analytical Chemical Research Group (FQM 323)
Department of Physical and Analytical Chemistry
Universidad de Jaén
Campus Las Lagunillas edif. B3, Jaén 23071, Spain
A. Sánchez-Ruiz
Departamento de Química Inorgánica
Orgánica y Bioquímica
Facultad de Farmacia Universidad de Castilla-la Mancha Avda
Dr. José María Sánchez Ibañez, s/n, Albacete 02071, Spain

chemicals, known as photosensitizers (PS), to generate cytotoxic Reactive Oxygen Species (ROS) by energy or electron transfer from a long-lived excited state.[7] PDT has a multitarget mode of action for eradicating malignant cells, derived from the broad reactivity of ROS against a wide range of cell components (i.e., lipids, DNA, proteins or carbohydrates), which hinders the emergence of bacterial resistance and, thus, makes PDT an ideal alternative to conventional antibacterial treatment.[8] However, the photosensitizing ability of traditional PSs is severely inhibited by aggregation-induced quenching (ACQ) after PS accumulation within bacteria, leading to minor ROS production.[9] Therefore, if aggregation causes an efficiency penalty, Aggregated Induced Emission (AIE) appears as the solution to overcome this problem. Upon aggregation, AIE materials' (known as AIEgens) emissive and photosensitizing properties are enhanced.[10–12] In fact, these materials could be rationally designed to undergo aggregation under specific physiological conditions of the bacterial cell, increasing the efficiency and the selectivity of the PDT treatment.[13–16] Although there have been some studies of AIEgens with great potential for future preclinical and clinical translation (especially as photoanticancer agents),[17] their structure, based on conjugated (aromatic) systems, is usually associated with low stability, mutagenicity, and biocompatibility.[18,19]

Alternatively, several independent laboratories have reported the emission from non-conjugated unconventional chromophores such as polyamides, dendrimers, or amino acids.[20,21] This phenomenon, designated by Clustering-Triggered Emission (CTE), results from the aggregation of heteroatoms (N, O, S, and P) and/or unsaturated bonds (C═O, C═C, and C≡N) and leads to the formation of emissive clusters,[22–24] due to the intramolecular through-space interaction (TSI) between the n and π electrons that are in close proximity.[25–27] This concept disrupts the traditional luminescence paradigm by attributing light absorption and emission to the different clouds of electrons resulting from a cluster formed by intra- and/or inter-interaction within the system [22,24] rather than the typical electron conjugation through bonds. Hence, the considerable amount of research proving the similarity between excited states CTE and those of traditional chromophores and/or quantum dots suggests the possibility of additional phenomena occurring.[28] Thus, it is not too much of a stretch to think that some CTE materials (known as CTEgens in analogy to AIEgens) could generate long-lived excited states capable of generating ROS.

To validate this hypothesis, a CTE system, specifically a carvone-based biomass polymer, was selected in this study. The utilization of biomass polymers will serve 2 principal functions: 1) It will reduce our reliance on non-renewable fossil-based carbon, and 2) it will facilitate the generation of novel materials with new functionalities.[29] Polyesters among biomass polymers are worthy of particular attention due to the electron-rich groups in their chains, which are essential for the formation of emission clusters. In light of recent findings on biomass-based CTEgen materials, specifically poly(PA-alt-COExo) developed by our group,[21] this polymer is a promising starting point for exploring other potential CTE mechanisms, such as ROS generation. The results are a significant milestone in the production of PSs, as they provide the first conclusive evidence that CTE-excited states can contribute to the generation of ROS. The principle has not only been validated spectroscopically, but it has also been used as a photoantimicrobial agent against Gram-positive *Staphylococcus aureus* bacteria. Finally, the results undoubtedly demonstrated that while this carvone-based polymer is non-toxic in the absence of light, its photoantimicrobial effect on the bacteria is significantly enhanced. It Is evident that this ROS generation is associated with CTEgens, as this phenomenon cannot be attributed to structure-specific processes but rather correlates with the CTE mechanism. Therefore, it is clear that CTEgens can undertake processes previously thought to be the exclusive domain of traditional chromophores. This fact suggests that applications that were previously limited to conventional chromophores, such as photosensitization, could now be developed using CTEgens.

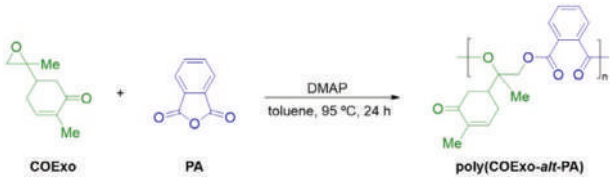

Figure 1. Synthesis of poly(PA-alt-COExo) according to reference.[21] DMAP = 4-dimethylaminopyridine.

2. Results and Discussion

2.1. Synthesis and Purity Assessment

It is crucial to recognize that the CTE mechanism is complex and frequently ambiguous, particularly because many substances with unexpected luminescence have been recently classified as CTEgens. This assignment was conducted without ensuring an exhaustive purification process to guarantee the absence of any impurities (e.g., multiple crystallization or sublimation purification steps). This is why, with increasing regularity, more studies have identified the role of impurities, whereby even at trace levels, the luminescence can be enhanced by up to 65%.[24,30] Accordingly, to preclude the possibility that impurities were the primary source of luminescence, all the reagents (carvone and phthalic anhydride) and solvents (toluene and dichloromethane) used in the synthesis process were sublimated and/or distilled on more than 3 occasions.

The synthesis of the polymer was developed according to a previously reported procedure (**Figure 1**).[21] Nevertheless, the absence of impurities in the solvents and reagents does not necessarily indicate the absence of such substances in the final product. Side reactions or incomplete reactions may form impurities, which could lead to erroneous conclusions. In this

A. Sánchez-Ruiz
Instituto de Biomedicina. Complejo de la Facultad de Medicina de Albacete
Universidad de Castilla-la Mancha
C/Almansa 14, Albacete 02008, Spain
C. Martín
Departmento de Química Física
Facultad de Farmacia
Universidad de Castilla-la Mancha
Avda. Dr. José María Sánchez Ibañez, s/n, Albacete 02071, Spain
E-mail: cristina.malvarez@uclm.es

regard, a highly sensitive method based on liquid chromatography–high-resolution mass spectrometry (LC–HRMS) was employed to detect the impurities at the trace level. Figure S1 (Supporting Information) shows the comparison between the Total Ion Chromatograms (TICs) for the polymer mixture and the blank control samples. Peaks between 13 and 19 min in the LC run were assigned to oligo(PA-alt-COExo)-related species; data from Table S1 (Supporting Information) shows the gradual incorporation of (PA-COExo) units to COExo, starting with one unit (m/z 521.2137) and reaching up to 7 units (m/z 2405.9100). Molecular ions in the detected peaks were a mixture of proton ($M+H^+$) and sodium ($M+Na^+$) adducts, with the latter being the most abundant one. Being the foundation upon which the higher-level oligomers were built, the structures of COExo-$(PA\text{-}COExo)_1$ and COExo-$(PA\text{-}COExo)_2$ were studied in detail through MS/MS experiments (Figure S2, Supporting Information), with the proposed structures for the observed fragments shown in table S2 and confirming the identity of the associated species. Since no COExo peak was observed in the TIC, and the rest of the peaks were related to these oligomeric structures with no presence of extraneous species, the LC-MS analysis provided strong evidence that the only source of the observed light-interacting mechanism (absorption, emission, or other relaxation processes), are the oligo(PA-alt-COExo)-related species.

2.2. Photophysical and Photochemical Properties

A dilute solution of carvone polymer in tetrahydrofuran (THF, a good solvent) appears colorless to the naked eye, showing neither absorption nor emission. However, when the concentration of the polymer is increased to over 0.1 g L^{-1}, the UV absorption undergoes a subtle change, exhibiting a tail extending into the visible region and becoming emissive in the blue/green region of the spectrum (**Figure 2**A). As previously reported, the phenomenon observed for this polymer is ascribed to the n,π^* and π,π^* electronic transitions that arise from the formation of different clouds of electrons of the through-space interaction generated clusters,[21] and is exacerbated by the presence of water (Figure 2B). When the water content exceeds 50% of v/v, the polymer starts to aggregate, changing the structure of the cluster. Under these conditions, a turbid suspension with a much brighter emission is obtained due to the more crowded structure of the aggregated polymer compared to neat THF (Figure 2C). To distinguish the absorption from the scattering component in the extinction spectrum, we recorded the absorption spectra using an integrating sphere, which minimizes the scattering component (Figure S3, Supporting Information). The absorption component also shows a strong absorption in the UV region with a tail extending into the visible region. However, its shape differs from that in THF, with more prominent absorption in the visible region and less intense in the UV-B/UV-C regions. This observation is consistent with the CTE mechanism, as the clusters are more densely packed in water, involving more electrons, and thus reducing the energy gap of the electronic transition. Notably, this redshift is also observed in the emission spectrum.

One question that can be addressed is whether these excited clusters can interact with oxygen to produce ROS. One of the

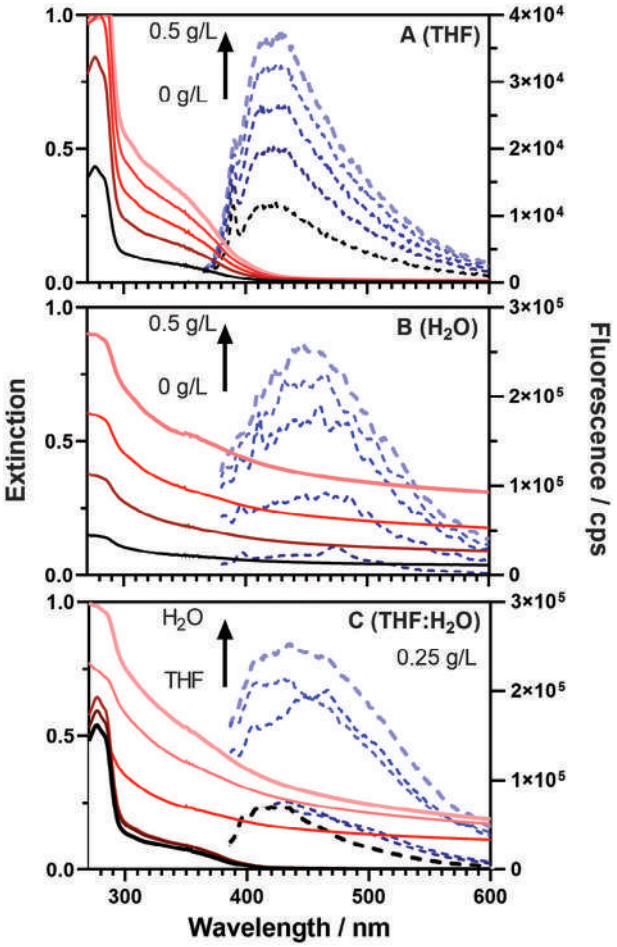

Figure 2. Extinction (red solid lines) and emission (blue dashed lines; λ_{Exc} = 355 nm) spectra of the polymer in THF (A; from 0 to 0.5 g L^{-1}, in increments of 0.1 g L^{-1}), H_2O (B; from 0 to 0.5 g L^{-1}, in increments of 0.1 g L^{-1}) and THF:H_2O mixtures (C; from neat THF to H_2O, in increments of 20% of H_2O content). The polymer concentration is 0.25 g L^{-1} in panel (C).

simplest methods for investigating this phenomenon is to monitor the production of singlet oxygen ($^1O_2$) by recording its weak NIR phosphorescence at 1275 nm (see Figure S4 (Supporting Information) for a detailed NIR spectral analysis). This spectroscopic fingerprint is a "gold standard" as it is specific to $^1O_2$ determination.[31] **Figure 3** shows the typical time-resolved emission of $^1O_2$ after nanosecond pulsed excitation of the polymer in THF and in H_2O (panels A,B respectively), where the $^1O_2$ production increases non-linearly with the polymer concentration (Figure S5, Supporting Information), which is characteristic of a CTE-mediated process. Moreover, this emission disappears when molecular oxygen is removed from the system by bubbling argon (Figure S4, Supporting Information). This process is highly efficient, as evidenced by the high $^1O_2$ production quantum yield (Φ_Δ = 0.45; Figure S6, Supporting Information), comparable to well-established clinically used PSs.[32] It is also noteworthy that this pathway is an order of magnitude more favorable than the emission of a photon by the cluster ($\Phi_F < 2 \times 10^{-2}$), highlighting the significant preference of this CTEgen material for the generation of long-lived excited states capable of generating ROS.

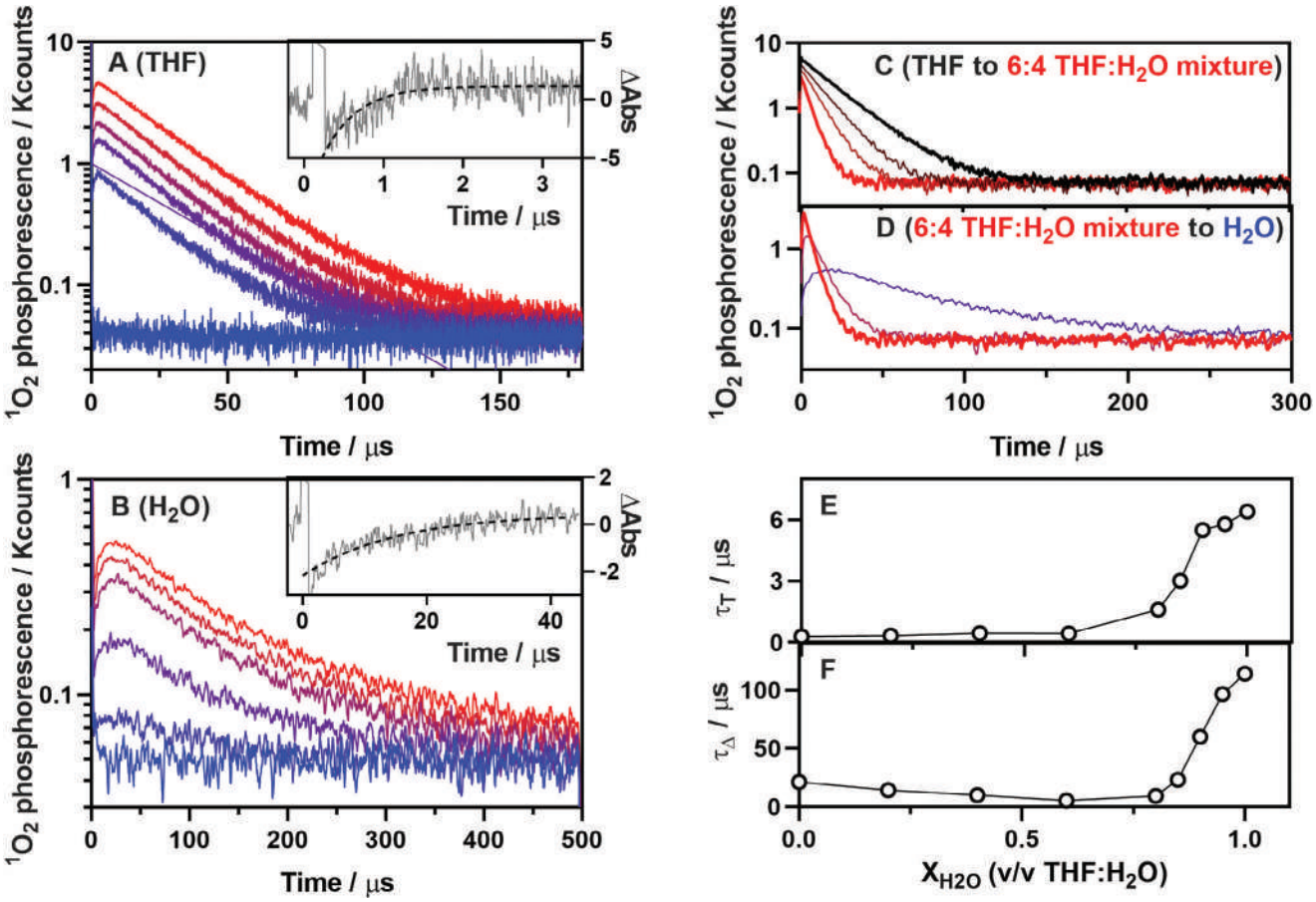

Figure 3. Singlet oxygen phosphorescence kinetic analysis. A,B): $^1O_2$ phosphorescence kinetic traces of the polymer in THF A) and H_2O (B), where the polymer concentration range was varied from 0 to 0.5 g L^{-1} in increments of 0.1 g L^{-1}. The insets in both figures depict the transient absorption traces of ground state bleaching recovery (λ_{exc} = 355 nm; λ_{obs} = 380 nm) at a polymer concentration of 0.5 g L^{-1}. C,D): $^1O_2$ phosphorescence kinetic traces of the polymer from black to red and from red to blue) in increments of 10% of H_2O content. The polymer concentration was 0.5 g L^{-1}. (E,F): Comparison of the triplet state (τ_T; E) and $^1O_2$ decay (τ_Δ; F) lifetimes with increasing the water content in the THF:H_2O solvent mixtures.

Notably, with impurities ruled out (Figures S1 and S2, Supporting Information), the observed $^1O_2$ phosphorescence is directly attributed to the excitation of these clusters.

The time-resolved $^1O_2$ phosphorescence signals provide additional insight into the formation and fate of $^1O_2$. In THF, the kinetic traces of $^1O_2$ show rise and decay lifetimes of 0.3 and 20 μs, assigned to the lifetimes of the $^1O_2$ precursor, namely the triplet state of the cluster (τ_T), and of $^1O_2$ (τ_Δ), respectively (Figure 3A). Indeed, the long-lived CTE excited state formation was confirmed by transient absorption experiments in which the ground-state cluster absorption recovers within a lifetime of 40 μs in deoxygenated samples and 0.3 μs in air-saturated solutions (Figure 3A inset; Figure S7, Supporting Information). Indeed, the equivalence of the τ_T decay lifetime observed by transient absorption spectroscopy with the rise lifetime recorded in $^1O_2$ phosphorescence strongly supports that the triplet state of the cluster is the immediate precursor of $^1O_2$ formation. Two main additional observations can be made from here: a) the τ_T is slightly longer than established conventional photosensitizers (typically around τ_T of 0.2 μs)[41] with a bimolecular quenching rate larger than 1×10^9 M^{-1} s^{-1} (Figure S7, Supporting Information), and b) the τ_Δ rises upon increasing the polymer concentration (Figure S8, Supporting Information). The initial observation is related to the fact that the oxygen accessibility to the cluster is slightly hindered, as well as the occurrence of both dynamic and static quenching, as evidenced by the non-linearity of the Stern-Volmer plot. The latter may be attributed to the preferential diffusion of the generated $^1O_2$, which can preferentially diffuse along the polymer chain before it escapes from the polymer matrix. These two effects become more apparent when the polymer structure collapses and forms aggregates upon increasing the water concentration.

To verify this hypothesis, the formation and decay kinetics of $^1O_2$ generated by photoexcitation of the polymer clusters in different THF:H_2O (v/v) mixtures were measured (Figure 3 panels C and D). At low water concentration, τ_Δ decreases with increasing water content, as expected from the shorter τ_Δ in neat water than in neat THF ($\tau_{\Delta;H2O}$ = 3.3 μs; $\tau_{\Delta;THF}$ = 20 μs).[32] However, this observation is reverted (i.e., τ_Δ increases), when the water content exceeds a certain threshold. This fact is consistent with the observation that water induces polymer aggregation and, consequently, a stronger and more tightly-packed clusterization.[21] It is, therefore, not surprising that the kinetic profile of $^1O_2$ phosphorescence is altered, with both lifetimes

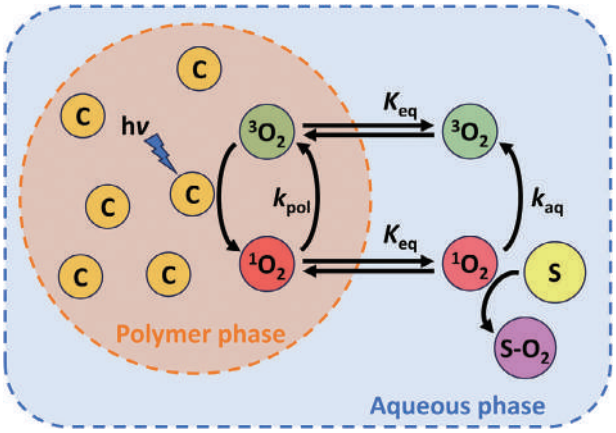

Figure 4. Description of the heterogeneous polymer suspension in water. Schematic description of the polymer and aqueous phases, including all the steps in which the formation and decay of $^1O_2$ are involved. Legend: C: cluster, ET: Energy transfer, S: substrate, and S-O_2: Oxidized substrate.

being enlarged (Figure 3, panels E and F). Tight packing in the clusters hinders the diffusion of oxygen into the cluster and the escape of $^1O_2$ into the external aqueous environment. Thus, the decay rate of the cluster's excited state is reduced, as evidenced by the slower ground state bleaching recovery of the cluster observed after laser flash photolysis in air-saturated water (Figure 3B inset), and the decay of $^1O_2$ is also slowed down due to the fact $^1O_2$ diffusion within the polymer becomes the rate-determining step. This is confirmed by the slight variation τ_Δ upon deuteration of the aqueous phase (from 105 to 115 µs in H_2O and D_2O, respectively; Figure S9, Supporting Information), while τ_Δ in neat H_2O and D_2O are 3.3 and 68 µs, respectively.[34] Indeed, under this condition, the $^1O_2$ kinetic trace still obeys a monoexponential rise and decay profile, suggesting that a fast chemical equilibrium is achieved between the $^1O_2$ located inside and outside the polymer microenvironment.[35] Accordingly, in consideration of the kinetic model for $^1O_2$ decay in a heterogeneous medium developed by Rodgers et al.,[35] only a tiny fraction of $^1O_2$ (less than 3% of the total) is capable of escaping from the polymer matrix and entering the external aqueous phase (**Figure 4**; further details can be found in Figure S9 and Table S3, Supporting Information). Although this fraction is small, the $^1O_2$ escaping molecules can still be trapped by a $^1O_2$-selective fluorescent probe located at the aqueous phase and/or absorbed at the surface of the polymer phase, such as tryptophan (Figure S10, Supporting Information). Therefore, these $^1O_2$ escaping molecules will be the cytotoxic species responsible for the (photo)-antimicrobial activity (vide infra).

To get a more complete picture, the effect of polymer concentration on the CTE photophysics/photochemistry has been explored (Figures 2 and 3). As a starting point, the properties were studied in THF. While no absorption, fluorescence, or $^1O_2$ production could be observed at low polymer concentration (<0.1 g L^{-1}), non-linear enhancements were recorded upon increasing the polymer concentration. This phenomenon has previously been observed for AIEgens PSs, whereby the aggregation of the PS favors the population of both singlet and triplet excited states.[20–24] Even though it is not unprecedented for CTE processes to be interpreted in terms of AIEgens, a concentration-dependent behavior in the formation of singlet and triplet excited states should be observed to validate such mechanism. As shown in Figures S5, S8, and S11 (Supporting Information), the absorption, fluorescence, and $^1O_2$ production increase nonlinearly with the polymer concentration in both solvents. Moreover, higher polymer concentration leads to a lengthening of τ_T due to the formation of a dense polymer cluster network, which is less permeable to molecular oxygen,[36] and longer τ_Δ can be attributed to the decrease in the density of $^1O_2$ quenching sites along the polymer aggregates compared to neat water.[37] These results not only support a mechanism similar to that observed for AIEgens, but also strongly support the potential of this polymer to form cluster aggregates, where their long-lived excited states can transfer their energy to molecular oxygen to generate significant amounts of $^1O_2$. A detailed discussion of the 7 solid pieces of experimental evidence that support this statement is found in the Supporting Information.

2.3. Photodynamic Inactivation of Bacteria

Encouraged by the observed production of $^1O_2$, the photoantimicrobial capabilities of this polymer were evaluated against *Staphylococcus aureus* (*S. aureus* ATCC 29 213). *S. aureus*, a representative example of Gram-positive bacteria, was chosen as a pathogenic model to unravel the potential application of CTEgens materials for photoantimicrobial treatments.[38] To perform this experiment, the polymer, dissolved in a concentrated DMSO solution, was added to a bacterial suspension in PBS, ensuring the final DMSO concentration remained below 1%. Then, the bacterial cell suspensions were incubated in the dark at 37 °C for 30 min. Notably, 1% DMSO is neither cytotoxic nor photocytotoxic under the tested conditions (Figure S12, Supporting Information). After the incubation period, the suspension was divided into 2 fractions: one kept in the dark to assess the intrinsic toxicity of the polymer and one irradiated with different violet light fluencies (400 nm, 15 mW cm^{-2}; see spectrum in Figure S13, Supporting Information). We opted for 400 nm violet light irradiation instead of UV-A irradiation to minimize the potential UV-A phototoxicity (vide infra).

To our best delight, the irradiated sample exhibited strong, concentration-dependent photoantimicrobial activity at both light fluences tested (27 and 80 J cm^{-2}; **Figure 5**A). In contrast, the polymer only induced minor dark toxicity (<0.6 $\log_{10}$CFU), even at the highest concentration tested. Specifically, a remarkable viability reduction of 6 $\log_{10}$ colony forming units (CFU) reduction (99.9999%) was achieved at a concentration of 0.15 g L^{-1} (80 J cm^{-2}), whereas a reduction of at least ≥ 3 $\log_{10}$CFU reduction (99.9%) was observed under milder conditions. These values (3 and 6 $\log_{10}$CFU) are especially significant as they represent the threshold levels required for efficient disinfection and sterilization, respectively, according to hand hygiene guidelines.[39] It is noteworthy that violet light is slightly phototoxic (≈1 $\log_{10}$CFU reduction) for *S. aureus* at the highest fluence tested, in accordance with the current literature on blue light PDI.[40] This fact complicates the selection of a UV light source with a better spectral overlap with the absorption of the polymer, which should be considered in the next generation of CTEgens materials for PDT.

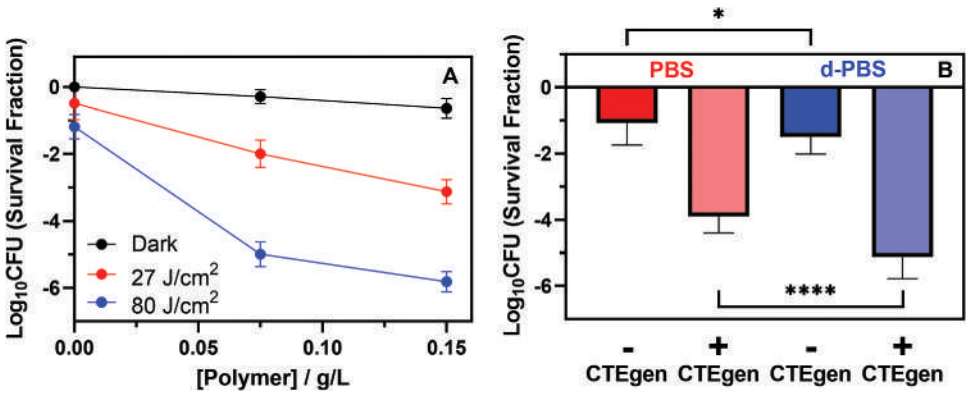

Figure 5. (Photo)-antimicrobial response of the polymer irradiated with violet light (400 nm). A): Survival curves of *Staphylococcus aureus* with different concentrations of polymer and irradiated with increasing violet light fluences (black, red, and blue lines for 0, 27, and 80 J cm^{-2}, respectively). B): Mechanistic studies of the photo-antimicrobial response in which *S. aureus* bacterial cells have been resuspended in PBS (red) or d-PBS (blue) in the absence (dark) or presence (light) of 0.15 g L^{-1} of polymer. The photodynamic treatment fluence is 27 J cm^{-2}. The symbols * and **** indicate p-values of $p \leq 0.05$ and $p \leq 0.0001$, respectively.

To identify the origin of the phototoxicity, the photoinactivation was repeated using the same bacteria suspended in deuterated phosphate buffer (d-PBS), which lengthens τ_Δ and, therefore, its photooxidative cytotoxicity. This is a commonly used control to evaluate the role of $^1O_2$ in PDT treatments.[34,41] Notably, in the absence of irradiation, replacing PBS with d-PBS does not show any significant cytotoxicity, indicating that d-PBS itself is not toxic to *S. aureus* (Figure S14, Supporting Information). Instead, light irradiation significantly increases phototoxicity both in the absence (*) or presence (****) of the polymer (Figure 5B). The increased phototoxicity in the absence of the polymer is consistent with the fact that blue/violet light is inherently toxic due to the presence of endogenous photosensitizers in bacteria. Since these endogenous PS are efficient $^1O_2$ PSs, their phototoxicity is enhanced in d-PBS due to the lengthening of the $^1O_2$ lifetime.[42] Therefore, to demonstrate the combined role of the polymer and d-PBS, we performed an alternative statistical analysis based on the difference in phototoxicity enhancement due to the presence of the CTEgen agent in PBS and d-PBS. To our delight, the phototoxicity enhancement due to the presence of the polymer is significantly larger in d-PBS than in PBS (****; Figure S15, Supporting Information). This finding proves that $^1O_2$ plays a key role in the photoinactivation of *S. aureus* by a CTEgen, in agreement with the abovementioned spectroscopic results.

Although these positive results motivated us to test the photoantimicrobial activity in 2 other pathogenic models of Gram-negative bacteria (*Escherichia coli* ATCC 35 218 and *Pseudomonas aeruginosa* ATCC 27 853),[43] no significant photoinactivation was observed (Figure S16, Supporting Information). This difference in activity prompted us to investigate how the non-charged polymer interacts with the 3 different bacteria. The cell walls of Gram-negative are more complex than those of Gram-positive bacteria because they have an external membrane outside the thin peptidoglycan layer. The main component of this outer membrane is lipopolysaccharide (LPS), which contains negatively charged sugars and phosphate. These components contribute to the cell surface's negative charge and act as a protective barrier, slowing the entry of toxic substances into the cell.[44] To study the interaction, we incubated the bacteria with 0.15 g L^{-1} of the polymer for 1 h, washed them, and then determined the presence of emissive clusters by resuspending the washed pellet in neat PBS (Figure S17, Supporting Information). The fluorescence of the clusters was stronger for *S. aureus* (Gram-positive) than for *E. coli* and *P. aeruginosa* (both Gram-negative). This finding suggests that more polymer aggregates interact with *S. aureus*, which is consistent with the slightly negative ζ-potential (indicative of the surface charge) of the aggregated polymer (-3.0 ± 0.6 mV) and with its higher phototoxicity against *S. aureus*. Moreover, the fluorescence band of the CTEgen material was red-shifted by 20–30 nm for all tested bacterial species compared to neat H_2O. This observation suggests that the interaction of the polymer with the surface of the external wall of bacteria alters the cluster geometry and structure, potentially tuning their photophysical and photosensitizing properties.

2.4. Outlook for Next Generation CTEgens Materials for Photodynamic Therapy

The experiments described above provide strong evidence from photophysical, photochemical, and photoantimicrobial perspectives that photoexcitation of CTEgens materials can efficiently produce $^1O_2$ (a type of ROS; see SI), supporting their potential use as photoantimicrobial agents. Typically, an ideal PS must meet 5 basic criteria for efficient photoinduced activity: i) it must absorb light efficiently, especially in the red/NIR region of the spectrum; ii) it should generate ROS with high quantum yield ($\Phi_{ROS} > 0.3$); iii) it should be resistant to photoinduced self-damage; iv) it should produce the ROS nearby the therapeutic target; and v) it should not be toxic under dark conditions.[7,45,46] Although the CTEgen reported in this work meets some of these criteria, such as high $^1O_2$ formation quantum yield and maintaining photoactivity after a PDT treatment of 80 J cm^{-2}, it does not excel in all areas. For example, it does not absorb red light, which limits its use to surface treatments only.[47] The value of this work lies in demonstrating that the excited state of CTEgens materials can explore deactivation pathways, such as energy transfer to

generate $^1O_2$, beyond emissive or internal conversion, as previously thought.[20,22,24,27] Notably, if the long-lived excited states of CTEgens materials can facilitate energy transfer processes, it could also potentially lead to other deactivation processes, such as electron transfer, resulting in the production of other ROS. This concept opens the door to expanding the potential applicability of CTEgens materials to other fields, such as PDT.

Improving the photophysical, photochemical, and phototoxic properties of CTEgens materials is a long-term endeavor. To rationally design the photosensitizing properties of these materials, we first need to understand their structure-property relationships and establish clear terminology for the overall TSI mechanism.[27,29] For example, other photosensitization mechanisms, such as spin-flip-based electron transfer observed in hyperbranched aliphatic polyaminoglycerol dendrimers, could also be partially related to CTE mechanism and expand our understanding of TSI-mediated phenomena.[48] Moreover, despite the challenges in accurately determining the structural and geometrical details of clusters involved in large CTE macromolecular systems, initial theoretical computational simulations have been recently reported. These simulations have calculated the CTE-emissive properties of different amino acids, serving as representative examples of small-molecule CTEgen materials, using molecular dynamics simulations.[49,50] Therefore, combining experimental and theoretical approaches will be beneficial for developing improved new generation(s) of CTEgens materials for PDT.

In addition to the efficiency of ROS production, the cellular uptake and localization of these CTEgens materials are also crucial due to the short range of action of the ROS generated.[6,51] A clear example is shown in this work, as the polymer aggregates effectively photoinactivated *S. aureus*, but were ineffective against *E. coli* and *P. aeruginosa*. This example is consistent with the stronger interaction of the polymer aggregates with Gram-positive bacteria due to the slightly negative ζ-potential of the polymer when it aggregates. In contrast, cationic photosensitizing agents with high hydrophilicity index are generally more effective against Gram-negative bacteria than neutral or anionic PS due to the negative net charge and higher complexity of their cell walls.[44,51] Future generations of CTEgen materials can be rationally designed with high biocompatibility and appropriate charge to precisely control cellular uptake and localization. This would be possible thanks to the wide variety of synthetic and natural polymers with CTE properties and the availability of versatile synthesis methods.[24] Moreover, post-functionalization can further fine-tune the cluster structure and the charge for specific applications.[52]

Finally, although we have only proved the use of CTEgens materials as photoantimicrobials, future generations of these materials could be applied in other fields, such as anticancer or antiviral treatments, where PDT has also proven effective.[53,54] Indeed, the CTE phenomena have been detected and described in various FDA/EMA-approved polymers used as excipients, drug delivery vehicles, or food additives. This fact suggests that in vitro CTE-based PDT treatments should have an accelerated translation to preclinical and clinical phases, thereby reducing the economic cost of the overall process by eliminating several regulatory steps.[55]

3. Conclusion

This work represents a turning point in the development of the next generation of PSs, as it is the first report to demonstrate that light excitation of CTEgen materials, such as this carvone-based polymer, can trigger long-lived excited states that could efficiently transfer their excess energy to molecular oxygen to produce ROS such as $^1O_2$. The novel mechanism outlined shows that CTEgens, together with their previously identified unique intrinsic luminescence, function in every respect as the well-described traditional chromophores. Furthermore, the demonstration of their high photoantimicrobial activity against a Gram-positive pathogenic bacterial model such as *S. aureus* laid the foundation for the generation of a new family of photosensitizers based on CTEgen materials. Taken together, these provide an excellent starting point for CTE-based PDT to address the current limitations of PDT, and to ensure long-term, effective healthcare with the most sustainable system possible.

4. Experimental Section

Synthesis of poly(PA-alt-COExo): In the glovebox, toluene (5 mL), 4-dimethylaminopyridine (DMAP) (31 mg, 254.5 µmol), carvone-based epoxide (COExo) (846 mg, 5.09 mmol) and phthalic anhydride (PA) (754 mg, 5.09 mmol) were placed into a 10 mL Schlenk equipped with a small stir bar. The Schlenk was then taken out of the glovebox and placed in a preheated oil bath under a nitrogen atmosphere at 95 °C for 24 h. Once the polyester was obtained, the viscous mixture was dissolved in the minimum amount of dichloromethane, precipitated with an excess of methanol, and, finally, filtered off and dried to constant weight to afford a white solid (1.47 g, 92%).

Characterization of Purity of poly(PA-alt-COExo): After appropriate dilution of the solid (1.12 mg of purified solid) was dissolved in 3 mL 1:1:1 (v/v/v) H_2O:MeOH:THF), Liquid chromatography coupled to high-resolution mass spectrometry (LC-HRMS) was employed for the analysis of artifacts and impurities. A UHPLC-Q-Orbitrap-MS/MS analysis was conducted utilizing a Vanquish UHPLC system (Thermo Fisher Scientific, Carlsbad, CA, USA) connected to a Q-Exactive mass spectrometer (Thermo Scientific) with heated electrospray ionization. The separation was conducted on a Zorbax Eclipse plus-C18 Rapid column (2.1 mm x 150 mm, 1.8 µm) (Agilent Technologies, Santa Clara, MA, USA). The mobile phase consisted of water A) and methanol B), both of which had 0.1% formic acid. A flow rate of 0.3 mL min^{-1} was selected, with a gradient starting at 10% B, then linearly increasing to 95% B at 17.0 min; remaining constant at 95% B until 5.0 min; decreasing to 10% B at 20.0 min; and being maintained constant for re-equilibration. The column was maintained at a temperature of 30 °C, and the injection volume was 1 µL.

The mass spectrum data was acquired in both positive and negative ion mode through full MS and higher energy collisional dissociation (HCD) data-dependent MS/MS by the UHPLC-Q-Orbitrap-MS/MS, which was equipped with a control software (Xcalibur, version 4.2.27). The scan parameters were set as follows: mass-to-charge ratio (m/z) scan range, 170 to 2500 Da; resolution, 70000; automatic gain control (AGC) target, 3×10^6; maximum injection time, 100 ms. The following parameters were employed for the heated electrospray ionization source (HESI source): spray voltage, 3.0 kV for ESI− and 3.5 kV for ESI+; sheath gas flow rate, 40 arb; auxiliary gas flow rate, 10 arb; sweep gas flow rate, 0 arb; capillary temperature, 320 °C; s-lens RF level, 50; and auxiliary gas heater temperature, 350 °C. A data-dependent scan (dd-MS2) was employed to obtain high-quality MS2 data. The 5 most intense precursors were automatically selected for MS/MS fragmentation by HCD. The parameters of the dd-MS2 method were as follows: resolution, 17500; AGC target, 2×10^5; maximum IT, 100 ms; loop count, 5; isolation window, 1 m z^{-1}. The Normalised Collision Energy (NCE) was set at 15 and 30 V.

Photophysical and Photochemical Characterization: All the solvents used for the photophysical and photochemical characterization have a spectroscopic grade or MiliQ water. UV–vis absorption spectra were recorded using a Varian Cary 6000i spectrometer (Varian, Palo Alto, CA, USA). Fluorescence emission spectra were recorded using a Spex Fluoromax-4 spectrofluorometer (Horiba Jobin-Ybon, Edison, NJ, USA).

$^1O_2$ generation was studied by time-resolved near-infrared phosphorescence using a customized Fluotime 200 time-resolved spectrophotometer (PicoQuant, Berlin, Germany).[31] A diode-pumped Nd:YAG laser (FTSS355-Q, Crystal Laser, Berlin, Germany) working at a 1-kHz repetition rate (0.5 µJ per pulse) was used for excitation at 355 nm. A 1064 nm rugate notch filter (Edmund Optics) and an uncoated SKG-5 filter (CVI Laser Corporation) were placed in the laser path to remove any residual NIR emission. The $^1O_2$ phosphorescence emitted by the sample was filtered with an 1100 nm long-pass filter (Edmund Optics) and later by a narrow bandpass filter at 1275 nm (BK-1270-70-B, bk Interferenzoptik). A thermoelectric-cooled NIR-sensitive photomultiplier tube assembly (H10330C-45-C3, Hamamatsu Photonics, Hamamatsu, Japan) was used as the detector. Photon counting was achieved with a multichannel scaler (TimeHarp 260 PICO board, PicoQuant, Berlin, Germany). The time dependence of the $^1O_2$ phosphorescence with the signal intensity S(t) is described by Equation 1, in which τ_T and τ_Δ are the lifetimes of the photosensitizer triplet state and of $^1O_2$, respectively, and S(0) is a preexponential parameter proportional to the $^1O_2$ formation quantum yield (Φ_Δ). For the methodology for determining Φ_Δ, please check Figure S6 (Supporting Information). The used reference photosensitizer is phenalenone ($\Phi_\Delta = 1$).[56]

$$(t) = S\,(0)\,x\left(\frac{\tau_\Delta}{\tau_\Delta - \tau_T}\right)x\left(e^{-t/\tau_\Delta} - e^{-t/\tau_T}\right) \quad (1)$$

Transient absorption kinetics (ΔAbs) were acquired using a home-built nanosecond laser flash photolysis system.[57] Briefly, the sample was excited by a 355 nm Q-switched Nd:YAG Laser (Surelite I-10, Continuum) with right-angle geometry. The analyzing beam is composed of a Xe lamp (PTI, 75 W) in combination with a dual-grating monochromator (mod. 101, PTI) coupled to a UV–vis radiation detector (PTI 710). The observation wavelength was selected to 380 nm, which corresponds to the ground state bleaching of the generated molecular clusters. The signal was fed to a Lecroy WaveSurfer 454 oscilloscope for digitizing and averaging (10 shots) and finally transferred to a PC for data storage and analysis.

Photoantimicrobial Studies: Three different strains, one gram-positive, *Staphylococcus aureus* (*S. aureus*, ATCC 29 213), and 2 gram-negative, *Escherichia coli* (*E. coli*, ATCC 35 218) and *Pseudomonas aeruginosa* (*P. aeruginosa*, ATCC 27 853) were used in this study. Briefly, the culture media used for growing the cells was Tryptic Soy Broth (TSB). The PDT treatment protocol was adapted from Reference [58]. The strains were grown overnight at 37 ± 1 °C in an orbital shaker at 60 rpm under aerobic conditions. Then, 100 µL of the culture was grown in 10 mL of fresh TSB until reaching an optical density of 0.18, measured at 600 nm. These OD_{600} values correspond to bacterial concentration of 10^7 CFU mL^{-1} for *S. aureus*, and 10^8 CFU mL^{-1} for *E. coli* and *P. aeruginosa*. After that, bacteria were harvested by centrifugation (4000 rpm, 10 min) and resuspended in the same volume of sterile PBS or deuterated PBS. Then, the adequate concentration of the polymer dissolved in DMSO (always ≤1%) was added to the bacterial suspension and incubated for 60 min in dark conditions. After, the bacterial suspension was irradiated using a violet LED (Figure S13, Supporting Information) until it reached the adequate light fluence (27 and 80 J cm^{-2}), using a light irradiance of 15.2 mW cm^{-2}. 1 mL of the bacterial suspension was kept unirradiated and used as the dark control. After the PDT treatment, the bacterial suspensions were diluted by a factor of 10 until reaching a 10^{-6} dilution factor. Finally, 10 µL of every dilution were spread on Tryptic Soy Agar and were incubated aerobically at 37 ± 1 °C. The colony-forming units (CFU) were counted after 24 h of incubation, and the dilution factor was considered.

To study the interaction between the CTEgen material and bacteria, the same 3 bacterial strains were used. The bacteria were grown until they reached an OD_{600} of 0.2. The bacteria were then harvested by centrifugation (4000 rpm, 10 min) and washed thrice with the same volume of sterile PBS. Next, the bacteria were incubated aerobically at 37 ± 1 °C for 1 h with CTEgen material at a concentration of 150 mg L^{-1}. The CTEgen was previously dissolved in DMSO, maintaining an overall DMSO concentration of 1%. To account for the autofluorescence of bacteria, control samples of each bacterium with 1% DMSO but without CTEgen were also incubated. After incubation, the cells were harvested by centrifugation, washed once, and resuspended in PBS. Finally, the fluorescence (λ_{Exc} = 355 nm) of the bacterial suspension for both the control samples and the samples incubated with CTEgen was measured.

Supporting Information

Supporting Information is available from the Wiley Online Library or from the author.

Acknowledgements

K.D.-P. and O.G. contributed equally to this work. The authors thank the MICIU/AEI projects refs. Grant numbers PID2020-115801RB-C22, PID2022-137569NA-C44, PID2021-12861OA-C22, PID2020-117788RB-I00, RYC2021-032773-I, CNS2022-136052, PID2023-149483NB-C22, and RED2022-134287-T) funded by MCIN/AEI/10.13039/501100011033 and FEDER, UE. This research was also supported by SBPLY/21/180501/000132, SBPLY/21/180501/000127, and SBPLY/23/180225/000094, funded by JCCM and the EU through "Fondo Europeo de Desarrollo Regional" (FEDER). This project has also received funding from the European Innovation Council (HORIZON EIC Grants; project number 101130615), by AGAUR (2020BP00066) and Universidad de Castilla-La Mancha (Grant 2021-GRIN-31240). S.N. thanks the Departament de Recerca i Universitats de la Generalitat de Catalunya for the support given to the research group (2021 SGR 01023) and the ICREA—Catalan Institution for Research and Advanced Studies for grant No. Ac2232308. The authors would also like to acknowledge the scientific support provided by Servicios Centrales de Apoyo a la Investigación (SCAI-UJAEN) from the University of Jaén and Dr. David Moreno González (University of Jaén) for this research project.

Conflict of Interest

The authors declare no conflict of interest.

Data Availability Statement

The data that support the findings of this study are available from the corresponding author upon reasonable request.

Keywords

biomass-derived polymers, cluster triggered emission, photodynamic therapy, reactive oxygen species, singlet oxygen

Received: August 14, 2024
Revised: December 9, 2024
Published online: December 25, 2024

[1] Centers for Disease Control and Prevention (CDC). *MMWR. Morbidity and Mortality Weekly Report* **1999**, *48*, 621.

[2] E. Commission, https://commission.europa.eu/document/download/9660deff-b855-443e-9fc7-597d58ce6879_en?filename=ec_rtd_he-partnerships-onehealth-amr.pdf&prefLang=es, (accessed: November 2024).
[3] W. H. Organization, https://www.who.int/news/item/27-02-2017-who-publishes-list-of-bacteria-for-which-new-antibiotics-are-urgently-needed, (Accessed: November **2024**).
[4] M. Miethke, M. Pieroni, T. Weber, M. Brönstrup, P. Hammann, L. Halby, P. B. Arimondo, P. Glaser, B. Aigle, H. B. Bode, R. Moreira, Y. Li, A. Luzhetskyy, M. H. Medema, J. L. Pernodet, M. Stadler, J. R. Tormo, O. Genilloud, A. W. Truman, K. J. Weissman, E. Takano, S. Sabatini, E. Stegmann, H. Brötz-Oesterhelt, W. Wohlleben, M. Seemann, M. Empting, A. K. H. Hirsch, B. Loretz, C. M. Lehr, et al., *Nat. Rev. Chem.* **2021**, *5*, 726.
[5] T. K. Burki, *Lancet Respir. Med.* **2021**, *9*, e54.
[6] M. Wainwright, T. Maisch, S. Nonell, K. Plaetzer, A. Almeida, G. P. Tegos, M. R. Hamblin, *Lancet Infect. Dis.* **2017**, *17*, e49.
[7] C. Hally, B. Rodríguez-Amigo, R. Bresolí-Obach, O. Planas, J. Nos, E. Boix-Garriga, R. Ruiz-González, S. Nonell, in *"Theranostics and Image Guided Drug Delivery"*, (Ed: M Thanou), RSC Publishing, London (UK) **2018**, 86–122.
[8] J. H. Correia, J. A. Rodrigues, S. Pimenta, T. Dong, Z. Yang, *Pharmaceutics* **2021**, *25*, 1332.
[9] J. Zhang, C. Jiang, J. P. Figueiró Longo, R. B. Azevedo, H. Zhang, L. A. Muehlmann, *Acta Pharm. Sin. B* **2018**, *8*, 137.
[10] J. Luo, Z. Xie, Z. Xie, J. W. Y. Lam, L. Cheng, H. Chen, C. Qiu, H. S. Kwok, X. Zhan, Y. Liu, D. Zhu, B. Z. Tang, *Chem. Commun.* **2001**, *18*, 1740.
[11] Z. Zhao, H. Zhang, J. W. Y. Lam, B. Zhong-Tang, *Angew. Chem., Int. Ed.* **2020**, *59*, 9888.
[12] H. Abrahamse, M. R. Hamblin, S. George, *Front. Chem.* **2022**, *10*, 984268.
[13] G. Feng, Y. Yuan, H. Fang, R. Zhang, B. Xing, G. Zhang, D. Zhang, B. Liu, *Chem. Commun.* **2015**, *51*, 12490.
[14] Y. Li, Z. Zhao, J. Zhang, R. T. K. Kwok, S. Xie, R. Tang, Y. Jia, J. Yang, L. Wang, J. W. Y. Lam, W. Zheng, X. Jiang, B. Z. Tang, *Adv. Funct. Mat.* **2018**, *28*, 1804632.
[15] X. He, Y. Yang, Y. Guo, S. Lu, Y. Du, J. J. Li, X. Zhang, N. L. C. Leung, Z. Zhao, G. Niu, S. Yang, Z. Weng, R. T. K. Kwok, J. W. Y. Lam, G. Xie, B. Z. Tang, *J. Am. Chem. Soc.* **2020**, *142*, 3959.
[16] Z. Liu, H. Zou, Z. Zhao, P. Zhang, G. G. Shan, R. T. K. Kwok, J. W. Y. Lam, L. Zheng, B. Z. Tang, *ACS Nano* **2019**, *13*, 11283.
[17] Z. Meng, H. Xue, T. Wang, B. Chen, X. Dong, L. Yang, J. Dai, X. Lou, F. Xia, *J. Nanobiotechnol.* **2022**, *20*, 344.
[18] J. Qian, B. Zhong-Tang, *Chem* **2017**, *3*, 56.
[19] Q. Borjihan, H. Wu, A. Dong, H. Gao, Y.-W. Yang, *Adv. Healthcare Mater.* **2021**, *10*, 2100877.
[20] S. Tang, T. Yang, Z. Zhao, T. Zhu, Q. Zhang, W. Hou, W. Z. Yuan, *Chem. Soc. Rev.* **2021**, *50*, 12616.
[21] F. de la Cruz-Martínez, R. Bresolí-Obach, I. Bravo, C. Alonso-Moreno, D. Hermida-Merino, J. Hofkens, A. Lara-Sánchez, J. A. Castro-Osma, C. Martín, *J. Mater. Chem. B* **2023**, *11*, 316.
[22] H. Zhang, B. Z. Tang, *JACS Au* **2021**, *1*, 1805.
[23] J. Liu, H. Zhang, L. Hu, J. Wang, J. W. Y. Lam, L. Blancafort, B. Z. Tang, *J. Am. Chem. Soc.* **2022**, *144*, 7901.
[24] R. Bresolí-Obach, J. A. Castro-Osma, S. Nonell, A. Lara-Sánchez, C. Martín, *J. Photochem. Photobiol. C: Photochem. Rev.* **2024**, *58*, 100653.
[25] S. T. Epstein, C. M. Rosenthal, *J. Chem. Phys.* **2008**, *64*, 247.
[26] H. Zhang, X. Zheng, N. Xie, Z. He, J. Liu, N. L. C. Leung, Y. Niu, X. Huang, K. S. Wong, R. T. K. Kwok, H. H. Y. Sung, I. D. Williams, A. Qin, J. W. Y. Lam, B. Z. Tang, *J. Am. Chem. Soc.* **2017**, *139*, 16264.
[27] P. Liao, J. Huang, Y. Yan, B. Z. Tang, *Mater. Chem. Front.* **2021**, *5*, 6693.
[28] J. Ge, M. Lan, B. Zhou, W. Liu, L. Guo, H. Wang, Q. Jia, G. Niu, X. Huang, H. Zhou, X. Meng, P. Wang, C. S. Lee, W. Zhang, X. Han, *Nat. Commun.* **2014**, *5*, 4596.
[29] Z. Wang, M. S. Ganewatta, C. Tang, *Prog. Polym. Sci.* **2020**, *101*, 101197.
[30] B. F. Laatsch, M. Brandt, B. Finke, C. J. Fossum, M. J. Wackett, H. R. Lowater, A. Narkiewicz-Jodko, C. N. Le, T. Yang, E. M. Glogowski, S. C. Bailey-Hartsel, S. Bhattacharyya, S. Hati, *ACS Omega* **2023**, *8*, 14208.
[31] A. Jiménez-Banzo, X. Ragàs, P. Kapusta, S. Nonell, *Photochem. Photobiol. Sci.* **2008**, *7*, 1003.
[32] F. Wilkinson, W. P. Helman, A. B. Ross, *J. Phys. Chem. Ref. Data* **1993**, *22*, 113.
[33] F. Wilkinson, W. P. Helman, A. B. Ross, *J. Phys. Chem. Ref. Data* **1995**, *24*, 663.
[34] P. R. Ogilby, C. S. Foote, *J. Am. Chem. Soc.* **1981**, *103*, 1219.
[35] P. C. Lee, M. A. J. Rodgers, *J. Phys. Chem.* **1983**, *87*, 4894.
[36] M. D. Groner, S. M. George, R. S. McLean, P. F. Carcia, *Appl. Phys. Lett.* **2006**, *88*, 051907.
[37] S. Hackbarth, S. Pfitzner, L. Guo, J. Ge, P. F. Wang, B. Röder, *J. Phys. Chem. C* **2018**, *122*, 12071.
[38] G. Y. C. Cheung, J. S. Bae, M. Otto, *Virulence* **2021**, *12*, 547.
[39] J. Boyce, D. Pittet, *Infect. Control Hosp. Epidemiol.* **2002**, *23*, 485.
[40] C. S. Enwemeka, T. L. Baker, V. V. Bumah, *J. Photochem. Photobiol.* **2021**, *8*, 100064.
[41] R. M. C. Di Martino, B. D. Maxwell, T. Pirali, *Nat. Rev. Drug Discovery* **2023**, *22*, 562.
[42] C. Treghini, A. Dell'Accio, F. Fusi, G. Romano, *Photochem. Photobiol. Sci.* **2021**, *20*, 985.
[43] C. L. Holmes, M. T. Anderson, H. L. T. Mobley, M. A. Bachman, *Clin. Microbiol. Rev.* **2021**, *10*, e00234.
[44] F. Liu, A. S. Y. Ni, Y. Lim, H. Mohanram, S. Bhattacharjya, B. Xing, *Bioconjugate Chem.* **2012**, *23*, 1639.
[45] M. Lan, S. Zhao, W. Liu, C.-S. Lee, W. Zhang, P. Wang, *Adv. Healthcare Mat.* **2019**, *8*, 1900132.
[46] T.-C. Pham, V.-N. Nguyen, Y. Choi, S. Lee, J. Yoon, *Chem. Rev.* **2021**, *121*, 13454.
[47] Z. Feng, T. Tang, T. Wu, X. Yu, Y. Zhang, M. Wang, J. Zheng, Y. Ying, S. Chen, J. Zhou, X. Fan, D. Zhang, S. Li, M. Zhang, J. Qian, *Light. Sci. Appl.* **2021**, *10*, 197.
[48] J. S. Nam, Y. Hong, C. G. Lee, T. I. Kim, C. Lee, D. H. Roh, I. S. Lee, S. Kweon, G. Ahn, S. K. Min, B. S. Kim, T. H. Kwon, *JACS Au* **2022**, *2*, 933.
[49] G. D. Mirón, J. A. Semelak, L. Grisanti, A. Rodriguez, I. Conti, M. Stella, J. Velusamy, N. Seriani, N. Došlić, I. Rivalta, M. Garavelli, D. A. Estrin, G. S. K. Schierle, M. C. G. Lebrero, A. Hassanali, U. N. Morzan, *Nat. Commun.* **2023**, *14*, 7325.
[50] G. Díaz-Mirón, C. R. Lien-Medrano, D. Banerjee, U. N. Morzan, M. A. Sentef, R. Gebauer, A. Hassanali, *J. Chem. Theory Comput.* **2024**, *20*, 3864.
[51] C. S. Oliveira, R. Turchiello, A. J. Kowaltowski, G. L. Indig, M. S. Baptista, *Free Radical Biol. Med.* **2011**, *51*, 824.
[52] R. A. J. Ditzler, A. J. King, S. E. Towell, M. Ratushnyy, A. V. Zhukhovitskiy, *Nat. Rev. Chem.* **2023**, *7*, 600.
[53] X. Li, J. F. Lovell, J. Yoon, X. Chen, *Nat. Rev. Clin. Oncol.* **2020**, *17*, 657.
[54] A. Wiehe, J. M. O'Brien, M. O. Senge, *Photochem. Photobiol. Sci.* **2019**, *18*, 2565.
[55] L. L. Osorno, A. N. Brandley, D. E. Maldonado, A. Yiantsos, R. J. Mosley, M. E. Byrne, *Nanomaterials* **2021**, *11*, 278.
[56] C. Marti, O. Jürgens, O. Cuenca, M. Casals, S. Nonell, *Photochem. Photobiol. A: Chem.* **1996**, *97*, 11.
[57] G. Bucher, R. Bresolí-Obach, C. Brosa, C. Flors, J. G. Luis, T. A. Grillo, S. Nonell, *Phys. Chem. Chem. Phys.* **2014**, *16*, 18813.
[58] R. Bresolí-Obach, I. Gispert, D. G. Peña, S. Boga, Ó. Gulias, M. Agut, M. E. Vázquez, S. Nonell, *J. Biophotonics.* **2018**, *11*, 201800054.